Probing nonlocal spatial correlations in quantum gases with ultra-long-range Rydberg molecules

J. D. Whalen,[1] S. K. Kanungo,[1] R. Ding,[1] M. Wagner,[2,3] R. Schmidt,[2,3] H. R. Sadeghpour,[4] S. Yoshida,[5] J. Burgdörfer,[5] F. B. Dunning,[1] and T. C. Killian[1,*]

[1]*Department of Physics and Astronomy and Rice Center for Quantum Materials, Rice University, Houston, Texas 77251, USA*
[2]*Max-Planck-Institute of Quantum Optics, Hans-Kopfermann-Straße 1, 85748 Garching, Germany*
[3]*Munich Center for Quantum Science and Technology, Schellingstraße 4, D-80799 München, Germany*
[4]*ITAMP, Harvard-Smithsonian Center for Astrophysics, Cambridge, Massachusetts 02138, USA*
[5]*Institute for Theoretical Physics, Vienna University of Technology, A-1040 Vienna, Austria, European Union*

We present photoexcitation of ultra-long-range Rydberg molecules as a probe of spatial correlations in bosonic and fermionic quantum gases. Rydberg molecules can be created with well-defined internuclear spacing, set by the radius of the outer lobe of the Rydberg electron wave function R_n. By varying the principal quantum number n of the target Rydberg state, the molecular excitation rate can be used to map the pair-correlation function of the trapped gas $g^{(2)}(R_n)$. We demonstrate this with ultracold Sr gases and probe pair-separation length scales in the range $R_n = 1400–3200\,a_0$, which are on the order of the thermal de Broglie wavelength for temperatures around $1\,\mu$K. We observe bunching for a single-component Bose gas of ^{84}Sr and antibunching due to Pauli exclusion at short distances for a polarized Fermi gas of ^{87}Sr, revealing the effects of quantum statistics.

Our understanding of quantum gases has been greatly enhanced by *in situ* measurements of spatial correlations, which can arise from Bose or Fermi quantum statistics [1–5] or formation of more complex entangled states [6–8]. Quantum-gas microscopes resolve correlations on length scales on the order of, or larger than, a wavelength of light, enabling studies of quantum magnetism [9] and the superfluid-to-Mott-insulator transition [10]. Inelastic loss from spin flips and three-body recombination probe two- and three-body spatial correlations at very short range [2,7]. Despite the tremendous progress in experimental techniques, *in situ* probes of spatial correlations between these length scales are lacking. Many complex many-body phenomena take place at these intermediate scales, and such a probe would provide a new window into the formation of halo dimers [11] and Efimov trimers [12], long-range Cooper pairs in strongly interacting Fermi gases [13,14], and strongly correlated one-dimensional gases [7,8].

Here we demonstrate photoexcitation of ultra-long-range Rydberg-molecule (RM) dimers [15–17] in an ultracold gas as an *in situ* probe of nonlocal pair correlations [1] at previously inaccessible length scales. At distances roughly equal to and smaller than the thermal de Broglie wavelength ($\lambda_{\mathrm{dB}} \sim 200$ nm), we observe bunching in a thermal gas of spinless bosonic ^{84}Sr and Pauli exclusion, or antibunching, in a polarized gas of fermionic ^{87}Sr atoms, reflecting the effects of (anti-)symmetrization of the wave functions dictated by the spin statistics theorem. Correlations vanish at distances greater than λ_{dB}. Bunching and antibunching have been observed before in quantum gases with destructive measurement schemes [2,5,18–21]. In contrast, RM excitation can be nearly nondestructive [22]. It can also probe the temporal evolution

of correlations since the molecular binding energy, and therefore the inverse excitation timescale, are much greater than the many-body energy scales of quantum gases, such as the Fermi energy or chemical potential.

In an RM dimer, one ground-state atom is bound to a highly excited Rydberg atom. The binding potential results from scattering between the Rydberg electron and ground-state atom [15,23], and it therefore follows the Rydberg-electron probability distribution (see Fig. 1). For Sr, the atom-electron interaction is attractive, leading to the formation of RMs. The molecular potential is also attractive for Rydberg excitations in Rb and Cs quantum gases [16,24,25], which attests to the broad applicability of the probe we investigate in the present work.

To probe spatial correlations, we exploit the fact that the internuclear separation in the most deeply bound RM dimer state, $|\chi_n^{\nu=0}\rangle$, is highly localized in the potential minimum formed by the outer lobe of the Rydberg wave function located at a separation $R_n \approx 2(n - \delta)^2 a_0$ (Fig. 1). The quantum defect is $\delta = 3.37$ for the $5sns\,^3S_1$ states used in this work, and $a_0 \approx 0.05$ nm is the Bohr radius. In a simple semiclassical picture, the formation of a molecule requires the presence of atoms separated by approximately R_n. Thus the excitation rate serves as a measure of the relative probability of finding two particles with separation R_n in the initial gas, which can be quantified by the nonlocal pair-correlation function $g^{(2)}(R_n)$. For principal quantum numbers n between 20 and 75, R_n ranges from 400 to $10^4 a_0$, providing an *in situ* probe of correlations at previously inaccessible length scales. This method is similar to the mapping of short-range ($\lesssim 100a_0$) atomic scattering states with photoassociative spectroscopy of low-lying energy levels [26–30]. The possibility of measuring nonlocal correlations with RMs was mentioned in [31], and short-range correlations were probed with RM excitation in [22].
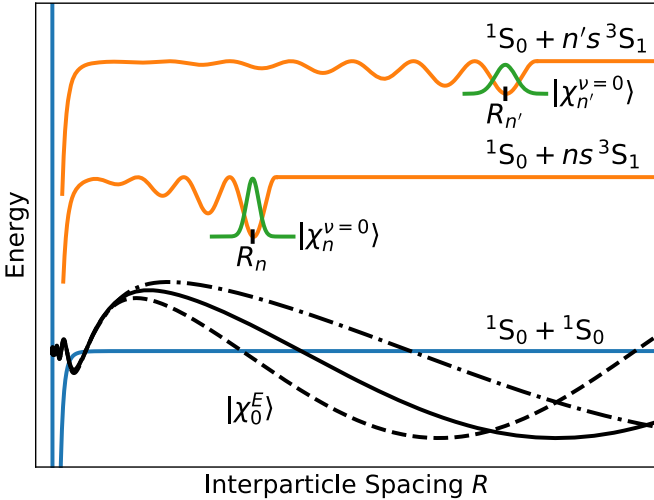
*Corresponding author: killian@rice.edu

FIG. 1. Schematic of the excitation to a Rydberg molecular state $|\chi_n^{\nu=0}\rangle$ (green) in a Rydberg potential (orange) from the state of a pair of colliding atoms $|\chi_0^E\rangle$ (black). The wave function of the ground $\nu = 0$ molecular dimer state is highly localized in the outer lobe of the molecular potential at R_n, as shown for two different principal quantum numbers n and n'. Asymptotically far outside the short-range interatomic potential (blue), $|\chi_0^E\rangle$ describes a free particle state with wave vector $k = \sqrt{2\mu E/\hbar^2}$ for collision energy E and reduced mass μ. The experiment samples a thermal distribution of collision energies (represented by the different $|\chi_0^E\rangle$ curves), and the molecular excitation rate is proportional to the pair-correlation function $g^{(2)}(R_n)$.
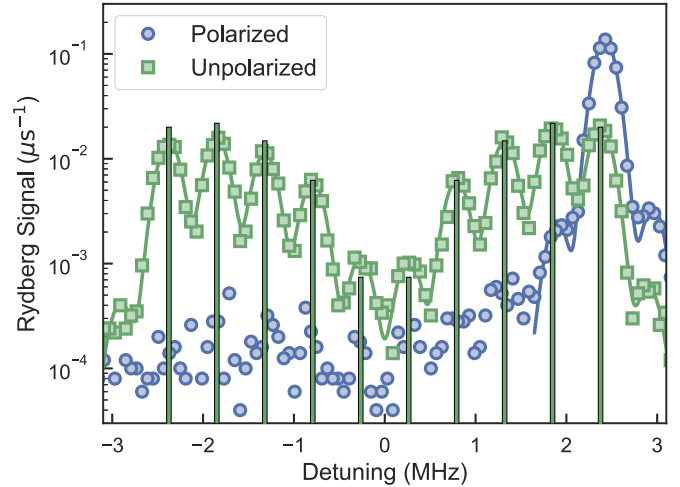

FIG. 2. Spectra for excitation to the $n = 34$ atomic Rydberg state for spin-polarized (circles) and unpolarized (squares) gases of ^{87}Sr. A 1 G magnetic field causes the observed Zeeman splitting. The vertical bars indicate the square of the product of Clebsch-Gordan coefficients associated with each transition, and differences with the measured peak heights point to small deviations from an equal distribution of m_F levels in the ground state. Curves show fits used to extract the population in each m_F level. Small features on the extreme right and left of the plot arise due to imperfect polarization of the first photon.

In the present work, nondegenerate quantum gases of spin-polarized, fermionic ^{87}Sr ($I = 9/2$) and bosonic ^{84}Sr ($I = 0$) are used to measure the effects of quantum statistics on the excitation rate of RMs and thus on the pair-correlation function. As a reference for quantitatively extracting $g^{(2)}(R)$, we employ an unpolarized sample of ^{87}Sr, which provides a good approximation to a gas of uncorrelated particles because of its tenfold-degenerate ground state. A preliminary discussion of the fermion data was presented in [32].

Atoms are laser cooled, loaded into an optical dipole trap (ODT) formed using 1064 nm light, and evaporatively cooled as described in [32]. Evaporative cooling of ^{87}Sr is performed with ^{84}Sr present in the trap for sympathetic cooling. For measurements involving spin-polarized ^{87}Sr, a bias magnetic field of 7.6 G is applied after loading the ODT, which produces a Zeeman splitting of $\sim$650 kHz between adjacent magnetic sublevels in the $5s5p\,^3P_1$ $F = 9/2$ manifold. Before evaporative cooling, population is transferred into the $m_F = 9/2$ ground state by applying a series of σ^+ polarized 689-nm laser pulses approximately 50 kHz red-detuned from each $m_F \rightarrow m_F + 1$ transition. Once this optical pumping is complete, the field is lowered to $\sim$1 G to maintain the quantization axis. Experiments with unpolarized samples are performed in zero magnetic field. For all ^{87}Sr experiments, once the final temperature is reached, any remaining ^{84}Sr atoms are removed by scattering light resonant with the $5s^2\,^1S_0 \rightarrow 5s5p\,^3P_1$ transition. The isotope shift between ^{87}Sr and ^{84}Sr ensures that no significant heating of the ^{87}Sr atoms occurs.

A two-photon transition is employed to create Rydberg atoms or molecules. The first photon, at 689 nm, has a fixed blue-detuning of 14 MHz from the $5s5p\,^3P_1$ level ($F = 11/2$ for ^{87}Sr). The energy of the second photon, at 320 nm, is scanned to obtain spectra for excitation to $5sns\,^3S_1$ levels ($F = 11/2$ for ^{87}Sr) (Figs. 2 and 3). The excitation lasers are applied for 10 μs, after which an electric field is applied to ionize Rydberg excitations. Product electrons are counted using a microchannel plate detector. Typically, 1000 laser pulses at a single frequency are applied to each sample. Excitation rates are kept much less than one per laser shot to avoid Rydberg blockade effects (blockade radius $R_B = (C_6/2h\gamma)^{1/6} \sim 3.5$ μm at $n = 39$ for linewidth $\gamma = 300$ kHz and $C_6 = 7 \times 10^{-61}$ J m^6 [33]).

To quantitatively measure the pair-correlation function $g^{(2)}(R)$, the molecular excitation rate in a single-component gas is normalized with respect to the rate in an unpolarized ^{87}Sr gas. This allows us to cancel experimental factors and, most importantly, n-dependent contributions to the excitation rate that are unrelated to spatial correlations. Maintaining similar sample densities and temperatures increases the accuracy of this procedure. To this end, we approximately match the final trap potential, excitation laser intensity, atom number ($N \sim 2 \times 10^5$), peak density ($\rho \sim 3 \times 10^{13}$ cm^{-3}), and sample temperature. The latter quantities are inferred from time-of-flight absorption imaging on the $5s^2\,^1S_0 \rightarrow 5s5p\,^1P_1$ transition at 461 nm and knowledge of the trapping potential [34]. The final trap oscillation frequencies and rms cloud radii are approximately (125, 125, 300) Hz and (12, 12, 5) μm respectively, with the tight axis along gravity.

The effectiveness of optical pumping is measured spectroscopically through excitation of the $5sns\,^3S_1$ $F = 11/2$
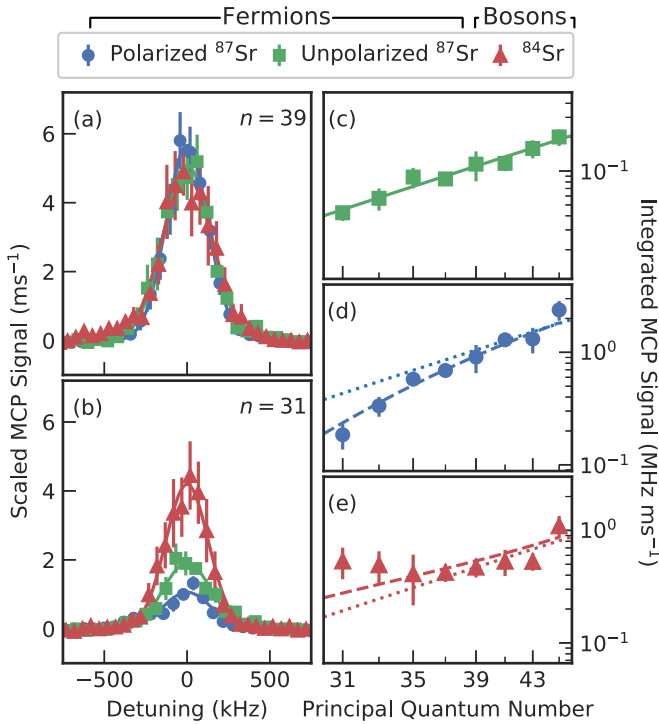
FIG. 3. Raw data showing the effects of quantum statistics on the excitation of RMs. (a),(b) Spectra for excitation to the $|\chi_n^{\nu=0}\rangle$ dimer ground state for a spin-polarized ^{87}Sr Fermi gas (blue, circles), for an unpolarized ^{87}Sr Fermi gas (green, squares), and a spinless ^{84}Sr Bose gas (red, triangles). The spectra for the polarized Fermi gas and the spinless Bose gas are scaled such that all spectra match at $n = 39$ to highlight the effects of quantum statistics at low n (see text). (c)–(e) Integral of the RM dimer spectra versus principal quantum number for (c) unpolarized ^{87}Sr, (d) polarized ^{87}Sr, and (e) ^{84}Sr. In (c), a fit (solid green line) shows that the integral for the unpolarized ^{87}Sr gas varies as $(n - \delta)^\alpha$, with $\alpha = 3.5(3)$. (d),(e) The dotted lines are translations of the $(n - \delta)^\alpha$ curve, and dashed lines are theory predictions accounting for quantum statistics and the n-dependent structure of Rydberg molecular wave functions.

atomic Rydberg state in a 1 G magnetic field using two π-polarized photons ($\Delta m_F = 0$). The spectrum (Fig. 2) is fit to a line shape model to determine the degree of polarization. For a polarized sample, at least 90% of the atoms occupy the $m_F = 9/2$ state. For the unpolarized Fermi gas, the populations in the ten different ground-state m_F levels are approximately equal ($\pm 25\%$). Differing heights of the Zeeman peaks in the spectrum for the unpolarized sample arise from the variation of transition strength from the ground state to final states with different magnetic quantum numbers as given by angular momentum coupling (Clebsch-Gordan coefficients).

To probe spatial correlations and measure $g^{(2)}(R)$, a polarization configuration different from the one used to probe polarization is used to create Rydberg molecules. The first photon is σ^+ polarized, and the second photon remains π polarized, which maximizes the transition strength for the spin-polarized sample.

The influence of quantum statistics on spatial correlations is apparent in the spectra for excitation to the $\nu = 0$ RM state

at principal quantum numbers $31 \leqslant n \leqslant 45$ ($1400 \, a_0 \leqslant R_n \leqslant 3200 \, a_0$). Figures 3(a) and 3(b) show spectra for $n = 31, 39$. The spectra for the spin-polarized Fermi gas ($T = 860$ nK) and Bose gas ($T = 650$ nK) are scaled such that their integrals match the integral of the unpolarized data ($T = 860$ nK) at $n = 39$, where the effects of quantum statistics are small [Fig. 3(a)]. With decreasing quantum number [Fig. 3(b)], the suppression of the excitation rate in the spin-polarized Fermi gas arising from Pauli exclusion and the enhancement for the Bose gas due to bunching are evident.

Figures 3(c)–3(e) include the integral of the molecular signal measured for each n for (c) unpolarized ^{87}Sr, (d) polarized ^{87}Sr, and (e) ^{84}Sr. The integrals for the unpolarized Fermi gas can be fit well by an $(n - \delta)^{3.5}$ power law (solid green line). This agrees well with the approximate $(n - \delta)^{3.8}$ scaling predicted using numerical calculations of the overlap integral between scattering and molecular states and the $1/(n - \delta)^3$ scaling of the electronic dipole transition matrix element. In Figs. 3(d) and 3(e), the dotted lines vary as $(n - \delta)^{3.5}$ and are scaled to match the polarized ^{87}Sr and ^{84}Sr data at high quantum number. In the absence of effects of quantum statistics, the integrals for all samples should have the same n dependence but different overall amplitudes that reflect n-independent factors such as Clebsch-Gordan coefficients (Fig. 2), differences in detector efficiency arising from the magnetic field needed to preserve quantization for the spin-polarized sample, and small differences in laser intensity between the Bose and spin-polarized Fermi gas experiments. Deviations from the $(n - \delta)^{3.5}$ power law at low quantum number result from quantum statistics.

The excitation probability to the ground vibrational state ($\nu = 0$) of the RM for principal quantum number n is proportional to a Franck-Condon factor that accounts for a thermal average over collision energy ($\langle \cdots \rangle_E$) for initial two-particle states and all possible initial and final rotational states. This reduces to $\mathcal{F}_n = \sum_l (2l + 1) \langle | \int dR \, R^2 \chi_n^{\nu=0}(R) \chi_0^{E,l}(R)|^2 \rangle_E$, where $\chi_n^{\nu=0}$ is the radial wave function for the RM, which is independent of l for the low-l states contributing to $\mathcal{F}_n$. $\chi_0^{E,l}$ is the wave function for the initial state with collisional energy E and rotational angular momentum quantum number l. To account for quantum statistics, the sum over l is understood to be restricted to initial states with allowed exchange symmetry. This yields the theory curves in Figs. 3(d) and 3(e) (dashed lines), which are in reasonable agreement with the data.

$\chi_n^{\nu=0}$ is well localized at R_n on the scale of the initial collisional state. In particular, the wave function for $n < 50$ is localized within a single potential well (Fig. 1). This allows $\mathcal{F}_n$ to be approximated as

$$\mathcal{F}_n \simeq \left| \int dR \, R^2 \chi_n^{\nu=0}(R) \right|^2 g^{(2)}(R_n) \equiv \mathcal{O}_n \, g^{(2)}(R_n), \quad (1)$$

where $g^{(2)}(R_n)$ is the pair-correlation function for separation R_n, and $\mathcal{O}_n$ is an effective Franck-Condon factor. This derivation can be generalized to the case of an initial state of a many-body Fermi or Bose gas at arbitrary density and temperature and with multiple internal spin states initially populated.

When experimental factors are taken into account, the integrated signal becomes

$$\mathcal{S}_n \simeq \alpha I_1 I_2 \mathcal{N} \beta_n C \mathcal{O}_n g^{(2)}(R_n), \quad (2)$$

which is proportional to the detector efficiency α, the two-photon-excitation laser intensities I_1 and I_2, the volume integral of the square of the density distribution $\mathcal{N} \equiv \int d^3r \, \rho(\mathbf{r})^2$, a factor β_n proportional to the square of the reduced two-photon electronic-transition matrix element, a factor C expressible in terms of Clebsch-Gordan coefficients, $\mathcal{O}_n$, and $g^{(2)}(R_n)$.

For nondegenerate gases of noninteracting particles, $g^{(2)}(R)$ is given by

$$g^{(2)}(R) = 1 + \epsilon e^{-2\pi R^2/\lambda_{\mathrm{dB}}^2}, \tag{3}$$

where $\lambda_{\mathrm{dB}} = h/\sqrt{2\pi m k_B T}$, and ϵ equals $+1$ (-1) for indistinguishable thermal bosons (fermions) in identical internal states and 0 for classical statistics [1,35]. Trap and phase-space-density-dependent corrections to Eq. (3) will vary with separation R and are always less than $z/10$ [1], where $z \approx \rho \lambda_{\mathrm{dB}}^3$ is the fugacity. The highest peak fugacity in these experiments is $z = 0.4$, and corrections are small. Equation (3) neglects interactions between ground-state particles, which modify spatial correlations at length scales less than the scattering length or the range of the ground-state atom-atom molecular potential, which are less than R_n probed in this experiment.

Equation (2) is used to experimentally determine $g^{(2)}(R_n)$ for indistinguishable particles in identical internal states by normalizing the integrated signals for the bosons and spin-polarized fermions to the integrated signal for the unpolarized fermions. This cancels common factors β_n and $\mathcal{O}_n$. For the unpolarized Fermi gas, we assume $g^{(2)}(R) = 1 - 0.1e^{-2\pi R^2/\lambda_{\mathrm{dB}}^2}$, which is the generalization of Eq. (3) for equal populations in the ten ground spin states. Remaining factors that vary between different experimental runs and different isotopes and sample polarizations, are either measured or calculated independently. The Clebsch-Gordan factor for the unpolarized gas (C_{unpol}) is calculated assuming equal populations in all ground spin states, yielding $C_{\mathrm{pol}}/C_{\mathrm{unpol}} = 5.05$, where C_{pol} describes bosons and polarized fermions. Temperatures and densities of each sample and the unpolarized gas used for normalization match within 10% in all cases. For the Bose gas, $T/T_c \approx 1.5$ where T_c is the critical temperature for Bose-Einstein condensation. For the polarized Fermi gases, $T/T_F \approx 1.0$, where T_F is the Fermi temperature. For the unpolarized Fermi gases, $T/T_F \approx 2$. Density distributions are calculated using the appropriate Bose or Fermi distributions.

At large separations, where the effect of quantum statistics should be negligible, this procedure yields $g^{(2)}(R) = 1.5$ rather than the expected value of 1. A systematic deviation of this size is consistent with uncertainties in relative populations of the initial internal spin states of the unpolarized Fermi gas and in trap geometry and resulting density profiles. Ratios are thus divided by an additional correction factor of 1.5 to obtain the values of $g^{(2)}(R_n)$ in Fig. 4. At lower values of n the normalized integrated signals for the bosons and fermions clearly deviate from unity [Fig. 4(a)]. The boson signal increases while the fermion signal decreases, which is consistent with bunching and antibunching, respectively. The Fermi-gas experiment was performed at two different temperatures, and antibunching is less pronounced in the warmer sample
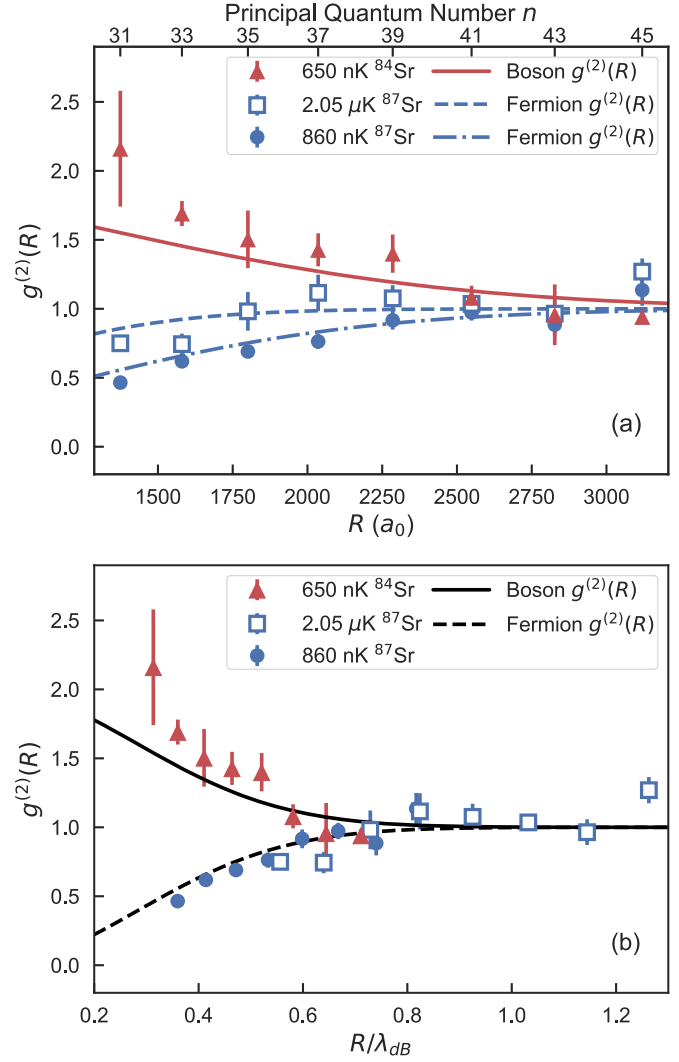

FIG. 4. Measured pair-correlation function for indistinguishable particles in identical internal states. (a) $g^{(2)}(R)$ for a Bose gas and Fermi gases at two different temperatures plotted against interparticle separation, R. Sample temperatures are indicated in the legend. (b) $g^{(2)}(R)$ for Fermi and Bose gases plotted against R scaled by the thermal de Broglie wavelength. The two sets of fermion measurements (blue symbols) fall onto a single curve and approach a constant value at large scaled distances. Error bars indicate statistical fluctuations from repeated measurements. Expected $g^{(2)}(R)$ [Eq. (3)] for bosons (solid) and fermions (dashed and dot-dashed) are shown by the lines.

reflecting the shorter thermal de Broglie wavelength. Figure 4 also shows that the results follow the expected behavior for $g^{(2)}(R)$ [Eq. (3)].

On a scaled, dimensionless axis [Fig. 4(b)], the two fermionic data sets fall on the same curve and approach a constant value for larger R/λ_{dB}. Effects of quantum statistics—bunching for bosons and antibunching due to Pauli exclusion for fermions—are strikingly evident.

In summary, we have demonstrated that photoexcitation of the most deeply bound, $\nu = 0$ dimer RM state provides an *in situ* probe of pair correlations in an ultracold gas that can be tuned over previously inaccessible length scales.

These results suggest other interesting phenomena that can be studied with this diagnostic. For example, the pair-correlation function in a gas with a large *s*-wave scattering length should show strong deviations from the noninteracting result presented in Eq. (3). Stronger suppression and enhancement effects on higher-order correlations should be observable with trimers, tetramers, etc. Moreover, due to the fact that Rydberg molecule formation takes place on a timescale (~ 1 μs) much faster than the relevant many-body dynamics of quantum gases, RMs hold promise for *in situ* probing of the time evolution of ensemble averages of correlations during the nonequilibrium dynamics following quantum quenches or in driven many-body systems.

[1] M. Naraschewski and R. J. Glauber, Phys. Rev. A **59**, 4595 (1999).

[2] E. A. Burt, R. W. Ghrist, C. J. Myatt, M. J. Holland, E. A. Cornell, and C. E. Wieman, Phys. Rev. Lett. **79**, 337 (1997).

[3] W. Ketterle and H.-J. Miesner, Phys. Rev. A **56**, 3291 (1997).

[4] M. W. Zwierlein, Z. Hadzibabic, S. Gupta, and W. Ketterle, Phys. Rev. Lett. **91**, 250404 (2003).

[5] A. Omran, M. Boll, T. A. Hilker, K. Kleinlein, G. Salomon, I. Bloch, and C. Gross, Phys. Rev. Lett. **115**, 263001 (2015).

[6] I. Bloch, J. Dalibard, and W. Zwerger, Rev. Mod. Phys. **80**, 885 (2008).

[7] B. Laburthe Tolra, K. M. O'Hara, J. H. Huckans, W. D. Phillips, S. L. Rolston, and J. V. Porto, Phys. Rev. Lett. **92**, 190401 (2004).

[8] T. Kinoshita, T. Wenger, and D. S. Weiss, Science **305**, 1125 (2004).

[9] A. Mazurenko, C. S. Chiu, G. Ji, M. F. Parsons, M. Kanász-Nagy, R. Schmidt, F. Grusdt, E. Demler, D. Greif, and M. Greiner, Nature (London) **545**, 462 (2017).

[10] W. S. Bakr, A. Peng, M. E. Tai, R. Ma, J. Simon, J. I. Gillen, S. Fölling, L. Pollet, and M. Greiner, Science **329**, 547 (2010).

[11] T. Köhler, K. Góral, and P. S. Julienne, Rev. Mod. Phys. **78**, 1311 (2006).

[12] C. Chin, R. Grimm, P. Julienne, and E. Tiesinga, Rev. Mod. Phys. **82**, 1225 (2010).

[13] E. Altman, E. Demler, and M. D. Lukin, Phys. Rev. A **70**, 013603 (2004).

[14] S. Giorgini, L. P. Pitaevskii, and S. Stringari, Rev. Mod. Phys. **80**, 1215 (2008).

[15] C. H. Greene, A. S. Dickinson, and H. R. Sadeghpour, Phys. Rev. Lett. **85**, 2458 (2000).

[16] V. Bendkowsky, B. Butscher, J. Nipper, J. P. Shaffer, R. Löw, and T. Pfau, Nature (London) **458**, 1005 (2009).

[17] B. J. Desalvo, J. A. Aman, F. B. Dunning, T. C. Killian, H. R. Sadeghpour, S. Yoshida, and J. Burgdorfer, Phys. Rev. A **92**, 031403(R) (2015).

[18] M. Schellekens, R. Hoppeler, A. Perrin, J. Viana Gomes, D. Boiron, A. Aspect, and C. I. Westbrook, Science **310**, 648 (2005).

[19] T. Jeltes, J. M. McNamara, W. Hogervorst, W. Vassen, V. Krachmalnicoff, M. Schellekens, A. Perrin, H. Chang, D. Boiron, A. Aspect, and C. I. Westbrook, Nature (London) **445**, 402 (2007).

[20] M. Yasuda and F. Shimizu, Phys. Rev. Lett. **77**, 3090 (1996).

[21] T. Rom, T. Best, D. van Oosten, U. Schneider, S. Fölling, B. Paredes, and I. Bloch, Nature (London) **444**, 733 (2006).

[22] T. Manthey, T. Niederprum, O. Thomas, and H. Ott, New J. Phys. **17**, 103024 (2015).

[23] E. Fermi, Nuovo Cimento **11**, 157 (1934).

[24] C. Bahrim, U. Thumm, and I. I. Fabrikant, J. Phys. B: At., Mol. Opt. Phys. **34**, L195 (2001).

[25] D. Booth, S. T. Rittenhouse, J. Yang, H. R. Sadeghpour, and J. P. Shaffer, Science **348**, 99 (2015).

[26] R. Napolitano, J. Weiner, C. J. Williams, and P. S. Julienne, Phys. Rev. Lett. **73**, 1352 (1994).

[27] E. R. I. Abraham, W. I. McAlexander, J. M. Gerton, R. G. Hulet, R. Côté, and A. Dalgarno, Phys. Rev. A **53**, R3713(R) (1996).

[28] E. Tiesinga, C. J. Williams, P. S. Julienne, K. M. Jones, P. D. Lett, and W. D. Phillips, J. Res. Natl. Inst. Stand. Technol. **101**, 505 (1996).

[29] C. Boisseau, E. Audouard, J. Vigué, and P. S. Julienne, Phys. Rev. A **62**, 052705 (2000).

[30] K. M. Jones, E. Tiesinga, P. D. Lett, and P. S. Julienne, Rev. Mod. Phys. **78**, 483 (2006).

[31] M. T. Eiles, Phys. Rev. A **98**, 042706 (2018).

[32] J. D. Whalen, R. Ding, S. K. Kanungo, T. C. Killian, S. Yoshida, J. Burgdörfer, and F. B. Dunning, Mol. Phys. (2019), doi: 10.1080/00268976.2019.1575485.

[33] C. L. Vaillant, M. P. A. Jones, and R. M. Potvliege, J. Phys. B: At., Mol. Opt. Phys. **45**, 135004 (2012).

[34] S. Stellmer, F. Schreck, and T. C. Killian, in *Annual Review of Cold Atoms and Molecules*, edited by K. W. Madison, K. Bongs, L. D. Carr, A. M. Rey, and H. Zhai (World Scientific, Singapore, 2014).

[35] D. S. Dean, P. Le Doussal, S. N. Majumdar, and G. Schehr, Phys. Rev. A **97**, 063614 (2018).